Dalton Transactions

Dynamic Article Links

Cite this: *Dalton Trans.*, 2011, **40**, 1175

www.rsc.org/dalton

PAPER

Novel single-source precursors for the fabrication of $PbTiO_3$, $PbZrO_3$ and $Pb(Zr_{1-x}Ti_x)O_3$ thin-films by chemical vapor deposition

Michael Veith,*[a,b] Michael Bender,[a] Tobias Lehnert,[a] Michael Zimmer[b] and Anette Jakob[c]

Received 12th July 2010, Accepted 4th November 2010
DOI: 10.1039/c0dt00830c

Lead titanate, lead zirconate, and lead zirconate titanate (PZT) films in the sub-µm-range were produced at temperatures around 400 °C using novel single-source precursors in a classical thermal CVD process. The design of two bimetallic alkoxide compounds, a lead titanate and a lead zirconate source with almost identical physical properties and complement miscibility, resulted in a new quasi-single-source PZT precursor, an azeotropic mixture that evaporates at 30 °C and at a pressure of 4×10^{-1} mbar. After thermal treatment at 650 °C, transparent (100)-oriented PZT films with remnant polarization of 20 µC cm^{-2} and a coercive field strength of 20 V μm^{-1} were achieved. An additional lead source is not required.

Introduction

The application of integrated ferroelectric thin-films in FeRAMs,[1] in microwave and high-frequency devices or in sensors[2] and actuators is a reason for the continual interest in these materials. Because of its high ferroelectric properties, lead zirconate titanate (PZT: $Pb(Zr_xTi_{1-x})O_3$) is one of the most promising materials so far.[3] Common deposition techniques for the generation of ferroelectric PZT thin-films are the sputtering-process,[4–6] the sol–gel process[7] and the chemical vapor deposition (CVD) process.[8–12] Usually, these techniques are based upon three sources,[13] one for each metal species. In the case of the sputtering technique, three different metal sources are used[6] whereas in the case of sol–gel deposition or CVD three different precursors are usually needed. Because of different electron affinities (sputtering) and different volatilities or hydrolysis speeds of the used precursors (CVD, sol–gel), it is difficult to obtain the exact stoichiometry of the mixed oxide phase. Especially regarding the amount of lead, problems arise because of the high volatility and the high diffusivity of its precursors and its ion. Thus, an additional lead source and furthermore a SiO_2 diffusion barrier on the substrate is mostly used to prevent the loss of lead.[14]

In the present work, a new approach for the production of PZT thin-films by CVD is used. By the use of a so-called "single-source precursor", the number of sources is reduced from three to one. According to the definition given in a publication prior to this,[15] in a gas phase (CVD) or solution process (sol–gel), a single-source precursor (SSP) is a molecular compound which contains all the necessary elements of the final product in a well-defined molecule. Depending on the molecular structure and the choice of "ligands", the volatility and the activation energy to initiate the reaction to the desired mixed oxide phase is tunable in a certain range.[16–18] During the last decades, several single-source precursors for lead titanate or lead zirconate thin-film fabrication were developed: In a series of publications the synthesis of non-volatile single-source precursors with different stoichiometries for the sol–gel process is described.[19–22] The CVD process, on the contrary, entails an important requirement on a single-source precursor: its volatility. Whereas the synthesis of a volatile lead zirconate precursor turned out to be straightforward, the synthesis of a volatile lead titanate precursor raised remarkable problems. Up to now, only Vaartstra *et al.* have reported about the synthesis of a volatile lead titanate precursor.[23]

Our approach was the development of two single-source precursors with almost identical physical properties, like melting point and sublimation or boiling point and complement miscibility to obtain a quasi-single-source precursor for the thermal CVD of PZT with the advantage of constituting deliberately the Ti/Zr proportion in the morphotropic phase diagram of PZT.

Experimental section

All manipulations, unless otherwise noted, were performed under a dry nitrogen atmosphere using standard Schlenk techniques. All solvents and alcohols were dried appropriately, distilled prior to use, and stored under dry nitrogen. Et_3PbCl was purchased from ABCR GmbH & Co. KG, $Ti(NEt_2)_4$ and $Zr(NEt_2)_4$ were prepared according to literature procedures.[24] Benzene-d_6 and toluene-d_8 were used as received. The ^1H and ^{13}C NMR spectra were recorded on a Bruker ACF (200 MHz) and a Bruker Avance 400 NMR spectrometer (400 MHz, H, H-COSY). Analytical data

[a]*INM - Leibniz Institute for New Materials gGmbH, Department of CVD/Biosurfaces, Campus D2 2, 66123 Saarbruecken, Germany. E-mail: michael.veith@inm-gmbh.de; Fax: +49 681 9300 223; Tel: +49 681 9300 273*

[b]*Inorganic and General Chemistry, Saarland University, Campus C 4 1, P. O. Box 151150, 66041 Saarbruecken, Germany*

[c]*Fraunhofer Institute for Biomedical Engineering, Ensheimer Straße 48, 66386 St. Ingbert, Germany*

were measured on a CHN-900 instrument from LECO and on a 720 ES from Varian (ICP).

Synthesis of $Et_3PbN(SiMe_3)_2$ (1)

Et_3PbCl (2.28 g, 0.007 mol) was dissolved in 20 mL of toluene, whereupon a solution of $LiN(SiMe_3)_2$ (1.15 g, 0.007 mol in 20 mL toluene) was added dropwise while stirring. After the addition had started, a white precipitate appeared. The reaction mixture was stirred overnight. Following filtration, the light brown filtrate was removed and the volatiles were removed *in vacuo* at room temperature. The remaining yellow viscous liquid was distilled at 115 °C and 0.01 mbar. The distillate, $Et_3PbN(SiMe_3)_2$, is a yellow lucent oil. Yield: 34%. $C_{12}H_{33}NPbSi_2$ (M_w = 454.7617 g mol^{-1}). **^{1}H NMR** (C_6D_6, 25 °C), δ = 0.14 (s, 18H, C***H***$_3$); 1.42 (t, 9H, C***H***$_3$); 1.68 (q, 6H, C***H***$_2$). **^{13}C NMR** (C_6D_6, 25 °C), δ = 6.05 (***C***H$_3$); 24.28 (***C***H$_2$(CH$_3$)); 13.06 (CH$_2$(***C***H$_3$)).

Synthesis of $Et_3Pb(O^tBu)Zr(O^tBu)_4$ (2)

To a solution of $Et_3PbN(SiMe_3)_2$ (5 mL, 14.51 mmol) in toluene (15 mL) one equivalent of $Zr(NEt_2)_4$ (5.37 mL, 14.51 mmol) was added while stirring. Upon dropwise addition of neat HO^tBu (6.87 mL, 72.49 mmol), the light orange solution became colorless. The reaction mixture was stirred for 30 min. After that, the solvent and by-products were subsequently removed at reduced pressure. The remaining light yellow oil was dissolved in 10 mL of toluene and 5 mL neat HO^tBu (52.75 mmol) was again added dropwise to finish the alcoholysis. The solution was stirred for 30 min at 25 °C before the solvents and by-products were removed at reduced pressure. The remaining product $Et_3Pb(O^tBu)Zr(O^tBu)_4$, a light yellow oil, was distilled at 30 °C and 0.01 mbar. The distillate is a colorless oil. Yield: 85.8%; $C_{26}H_{60}O_5PbZr$ (M_w = 751.1694 g mol^{-1}): C 39.56% (calcd. 41.57%), H 7.98% (calcd. 8.05%), Pb 27.58% (calcd. 27.58%), Zr 12.15% (calcd. 12.14%). **^{1}H NMR** (toluene-d$_8$, 25 °C), δ = 1.36 (s, 9H, C***H***$_3$); 1.37 (s, 36H, C***H***$_3$); 1.45 (t, 9H, C***H***$_3$); 1.63 (q, 6H, C***H***$_2$). **^{13}C NMR** (toluene-d$_8$, 193 K), δ = 34.55 (***C***H$_3$); 70.69 (***C***(CH$_3$)$_3$); 32.70 (***C***H$_3$); 75.28 (***C***(CH$_3$)$_3$); 25.86 (***C***H$_2$(CH$_3$)); 12.68 (CH$_2$(***C***H$_3$)).

Synthesis of $Et_3Pb(O^tBu)Ti(O^tBu)_4$ (3)

To a solution of $Et_3PbN(SiMe_3)_2$ (5 mL, 14.51 mmol) in toluene (15 mL) one equivalent of $Ti(NEt_2)_4$ (5.25 mL, 14.51 mmol) was added while stirring. Afterwards the same procedure was employed as for the zirconium compound **2**. The product $Et_3Pb(O^tBu)Ti(O^tBu)_4$, a light yellow oil, was distilled at 30 °C and 0.01 mbar. The distillate is a colorless oil. Yield: 85.9%; $C_{26}H_{60}O_5PbTi$ (M_w = 707.8294 g mol^{-1}): C 41.71% (calcd. 44.12%), H 8.13% (calcd. 8.54%), Pb 29.27% (calcd. 29.27%), Ti 6.50% (calcd. 6.76%). **^{1}H NMR** (C_6D_6, 25 °C), δ = 1.33 (s, 36H, C***H***$_3$); 1.28 (s, 9H, C***H***$_3$); 1.45 (t, 9H, C***H***$_3$); 1.63 (q, 6H, C***H***$_2$). **^{13}C NMR** (C_6D_6, 25 °C), δ = 34.89 (***C***H$_3$); 70.68 (***C***(CH$_3$)$_3$); 32.41 (***C***H$_3$); 79.94 (***C***(CH$_3$)$_3$); 25.92 (***C***H$_2$(CH$_3$)); 12.71 (CH$_2$(***C***H$_3$)).

Synthesis of the quasi-single-source precursors (4)

To obtain quasi-single-source precursors for the deposition of PZT films, the single-source precursors **2** and **3** were mixed at different ratios under a dry nitrogen atmosphere. The distillation temperature of all mixtures was found to be constant at 30 °C and 0.01 mbar. After stirring the mixtures for 30 min, they are ready to be used in the CVD process. NMR spectra showed no reaction between **2** and **3**.

CVD of the SSPs 2, 3 and 4

A schematic diagram of the CVD reactor, used to deposit the ferroelectric films, is shown in Fig. 1. Pressure sensor S1 monitors the pressure inside the stainless steel precursor-supply-line. Sensor S2 measures the pressure inside the reaction chamber made of glass. By opening vessel V2, the CVD reactor is flushed with nitrogen up to vessel V1. V1 opens the way for nitrogen or the gaseous precursor inside the reaction chamber and thus controls the precursor flow. The substrates are heated up to temperatures between 350 °C and 500 °C using a graphite cylinder inside the core of an inductive coil. The temperature is monitored and controlled by a thermocouple. The surface temperature is monitored by a pyrometer. The reaction chamber is evacuated by a vacuum pump at its outlet. A cold trap between the pump and the chamber prevents the by-products from travelling inside the pump. If V1 is completely closed, the base pressure p_{base} inside the chamber is 7×10^{-2} mbar. The precursor flow Δp_p is defined as: $\Delta p_p = p_{measured,\ V1\ open} - p_{base}$

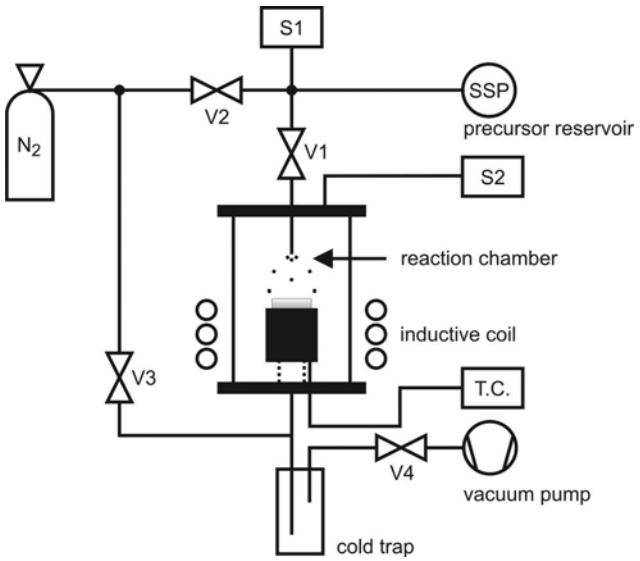

Fig. 1 Schematic diagram of the used vertical cold-wall CVD reactor. The precursor flow-rate is controlled by V1. The pressure is monitored by S1 and S2. The substrate-holder made of graphite is heated by an inductive coil and its temperature is measured and controlled by a thermocouple.

The chemical vapor deposition was carried out at different precursor-flows in the range from 0.4×10^{-1} mbar to 1.3×10^{-1} mbar.

Substrates

The substrates used were 0.5 mm thick, thermally oxidized SiO_2 (500 nm)/Si-wafers with a 150 nm Pt-electrode on a 20 nm Ti adhesive layer. The Pt electrodes were deposited using magnetron sputtering. They exhibited a (111) preferred orientation.[25]

Transformation to perovskite phase

After the deposition process, the coated substrates were thermally treated at temperatures between 500 °C and 700 °C for 5 min, using the rapid thermal annealing technique (RTA) to obtain the desired perovskite phase. The crystallization of the perovskite phase was observed by X-ray diffraction (XRD, Bruker AXS D8 Advance). Surface microstructures of the films were observed using a FEI (Quanta 400 ESEM FEG) field emission scanning electron microscope (SEM).

Patterning the perovskite films by wet etching

The obtained piezoelectric films were patterned using an etching technique described by Zheng *et al.*[26] Thus, several PZT dots with 1.5 mm diameter were fabricated.

Electrical characterization

The dielectric properties of the films (dielectric constant ε_r and dielectric loss δ) were measured with a precision LCR Meter (Agilent 4284A) after formation of an upper gold-electrode by sputtering. To display the ferroelectric hysteresis loop, a classical Sawyer–Tower circuit[27] was used while a modified PUND setup was used for the determination of the remnant polarization P_r.[28]

Results and discussion

$Et_3Pb(O^tBu)Zr(O^tBu)_4$ (2)

After mixing the educts $Et_3PbN(SiMe_3)_2$ and $Zr(NEt_2)_4$ in toluene, neat *tert*-butyl alcohol was added, whereupon the reaction mixture was stirred for 30 min. Instead of $Zr(NEt_2)_4$ or $Ti(NEt_2)_4$ also alcoholates like $M(O^iPr)_4$, M = Ti, Zr, may be used without any significant advantage in the yields or the products. NMR spectra of the reaction mixture showed no further reaction for the time after. Even after refluxing the mixture for several hours, no change was observed. Peaks of the educts, products and by-products identified as $HNEt_2$ and $HN(SiMe_3)_2$ were found. To shift the formed equilibrium to the product side, the by-products were subsequently removed at reduced pressure and the remaining reaction mixture was dissolved again in toluene, whereupon *tert*-butyl alcohol was added a second time. After a further 30 min stirring, the reaction to the product $Et_3Pb(O^tBu)Zr(O^tBu)_4$ was completed as concluded from NMR data and by-products were removed at reduced pressure. The equation for the reaction is summarized in (1).

$$\underset{\mathbf{1}}{Et_3PbN(SiMe_3)_2} + Zr(NEt_2)_4 \xrightarrow[\text{toluene}]{5\ HO^tBu} \underset{\mathbf{2}}{Et_3Pb(O^tBu)Zr(O^tBu)_4} + 4\ HNEt_2 + 1\ HN(SiMe_3)_2 \quad (1)$$

^{1}H NMR spectra for **2** show two overlapping singlets at 1.37 ppm, which can be ascribed to the *tert*-butoxy groups at the zirconium and the lead atom. The expected multiplets (t, q) of the ethyl groups are allocated over a range between 1.00 ppm and 2.00 ppm with central peaks at 1.45 ppm and 1.63 ppm. ^{13}C NMR spectra at 193 K show two broadened peaks at 34.55 ppm and at 32.70 ppm with a relative intensity of 1 : 4. We assigned the first one to the primary carbon atoms of a single *tert*-butoxy group at the lead atom. The second one is ascribed to the primary carbon atoms of four *tert*-butoxy groups at the zirconium atom. Furthermore, singlets at 25.68 ppm and 12.68 ppm were registered. Not only because of satellites of the ^1J-coupling ($^1J(^{13}C, ^{207}Pb)$ = 230.7 Hz) and the ^2J-coupling ($^2J(^{13}C, ^{207}Pb)$ = 30.5 Hz) with the lead atom, we assigned these resonances to the ethyl groups at the lead atom. Besides, the quaternary carbon atoms of the *tert*-butoxy groups at the zirconium atom cause a broadened peak at 75.28 ppm (193 K). The corresponding peak of the quaternary carbon atom at the lead atom is broadened likewise and to be found at 70.69 ppm (193 K). When the temperature is raised in the ^{13}C NMR from 193 K to 233 K, the separate signals for primary and quaternary carbon atoms merge. For example: at 233 K the signal of the primary carbon atoms of the *tert*-butyl groups is represented by a single line with δ = 33.01 ppm, which seems to indicate a coalescence phenomenon as the calculated δ value from the 193 K temperature (see above) is 33.01 ppm respecting the signal intensities of 1 : 4. Raising the temperature even higher (363 K) results in a reappearance of a broad peak at 34.89 ppm together with the dominant peak at 33.16 ppm. This could be an indication of a dissociative step to form Et_3PbO^tBu and $(^tBuO)_4Zr$. We assume that these broadened peaks as well as the coalescence are caused by interactions of the oxygen atoms of the *tert*-butoxy groups at the zirconium atom with the lead atom leading to an equilibrium. In Fig. 2, an equilibrium based upon the NMR data is shown in more detail. Clearly, a dynamic interchange of *tert*-butoxy groups seems to happen. In this model, all four *tert*-butoxy groups of the zirconium are engaged in the equilibrium. The structure on the left of Fig. 2 could be that found at 193 K in the NMR, whereas one of the transient species in the equilibrium is presented on the right. Because of the temperature dependent NMR spectra, we rule out independent molecules like Et_3PBO^tBu and $(^tBuO)_4Zr$ which on the other hand could easily form at elevated temperatures.

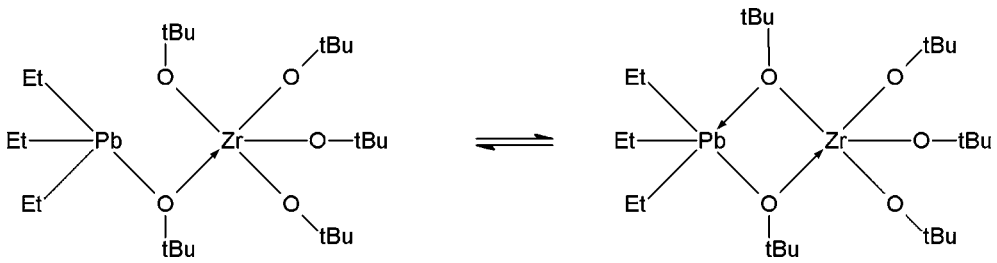

Fig. 2 Proposed equilibrium of $Et_3Pb(O^tBu)Zr(O^tBu)_4$ (**2**) in solution based upon NMR spectra.

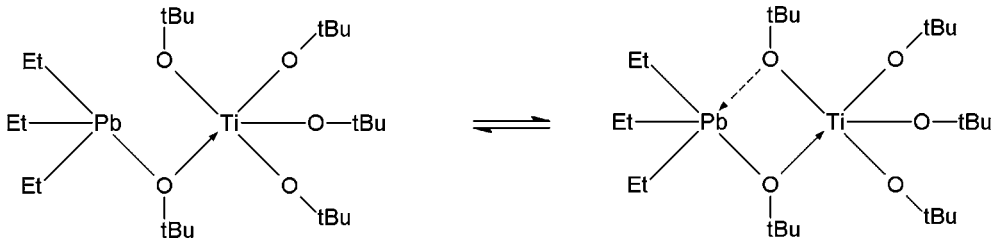

Fig. 3 Possible equilibrium of $Et_3Pb(O^tBu)Ti(O^tBu)_4$ (**3**) in solution.

$Et_3Pb(O^tBu)Ti(O^tBu)_4$ (3)

The synthesis of $Et_3Pb(O^tBu)Ti(O^tBu)_4$ was run in analogy to the synthesis of the corresponding zirconium derivate as may be seen from eqn (2).

$$\underset{\mathbf{1}}{Et_3PbN(SiMe_3)_2} + Ti(NEt_2)_4 \xrightarrow[\text{toluene}]{5\ HO^tBu} \underset{\mathbf{3}}{Et_3Pb(O^tBu)Ti(O^tBu)_4} + 4\ HNEt_2 + HN(SiMe_3)_2 \quad (2)$$

^{1}H NMR spectra of **3** show two well separated singlets at 1.33 ppm and 1.28 ppm with a relative intensity of 4 : 1. We assigned them to the *tert*-butoxy groups at the titanium atom and the lead atom. Resonances (multiplets) of the ethyl groups are allocated over a range between 1.00 ppm and 2.00 ppm with central peaks at 1.45 ppm (t) and 1.63 ppm (q), very similar to **2**. At room temperature, ^{13}C NMR spectra show two peaks at 34.89 ppm and 32.41 ppm with a relative intensity of 1 : 4. Because of the ^3J-coupling with lead ^{207}Pb (^3J (^{13}C, ^{207}Pb) = 17.88 Hz), the first one is ascribed to the primary carbon atoms of the *tert*-butoxy groups at the lead atom. The second peak is caused by the primary carbon atoms of four *tert*-butoxy groups at the titanium atom. Further peaks at 25.92 ppm and 12.71 ppm with satellites caused by the ^1J-coupling (^1J (^{13}C, ^{207}Pb) = 230.2 Hz) and by the ^2J-coupling (^2J, ^{13}C, ^{207}Pb) = 30.4 Hz) with the lead atom were assigned to

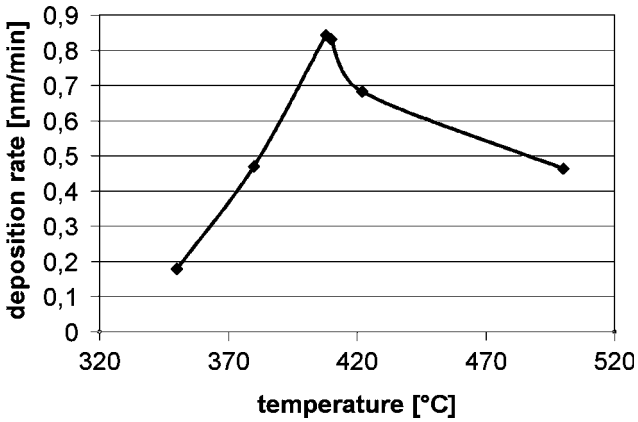

Fig. 4 Deposition rate for the CVD of **4** ($Et_3Pb(O^tBu)_5Ti/Et_3Pb(O^tBu)_5Zr$) at a constant precursor flow of 0.4×10^{-1} mbar and temperatures varying between 350 °C and 500 °C.

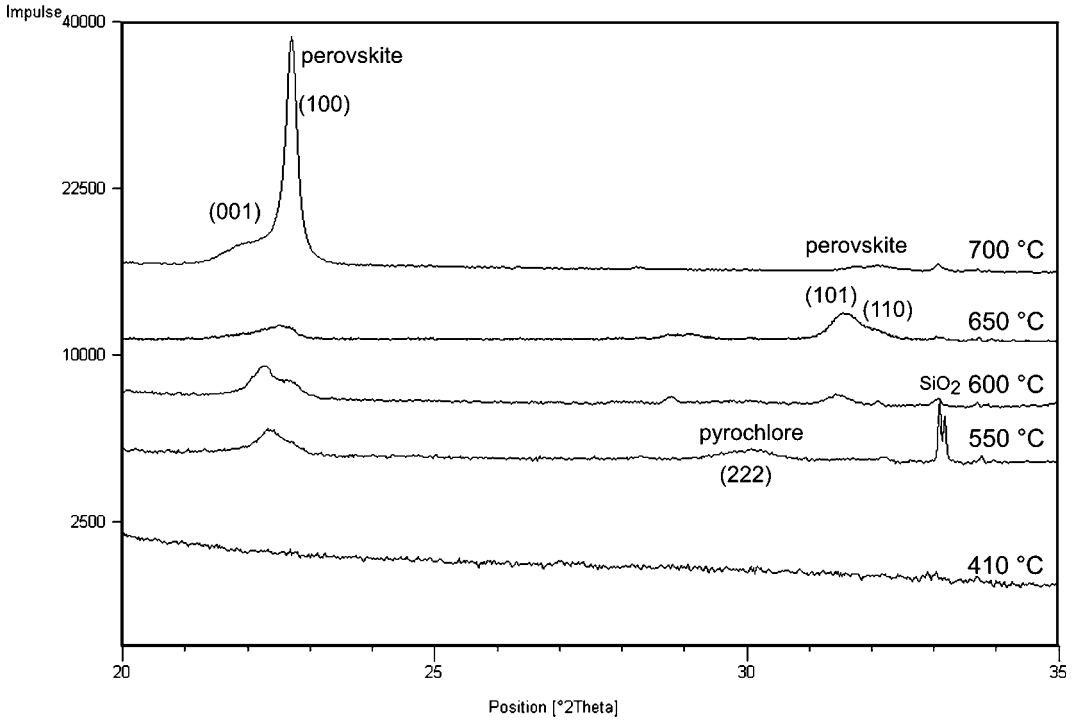

Fig. 5 XRD patterns of $Pb(Zr_{1-x}Ti_x)O_3$ films after RTA (rapid thermal annealing) treatment.

the ethyl groups at the lead atom. Besides, the quaternary carbon atoms of the *tert*-butoxy groups at the titanium atom cause a peak at 79.94 ppm. A peak at 70.68 ppm is caused by the quaternary carbon atom at the *tert*-butoxy group of the lead atom. Due to the ^{2}J-coupling with the lead atom, we found satellites at that resonance (^{2}J (^{13}C, ^{207}Pb) = 44.36 Hz). An equilibrium as found for **2** seems to be less prominent on the NMR time scale, but we cannot exclude it completely (Fig. 3). We also cannot exclude that only dissociated parts like Et_3PbO^tBu and $(^tBuO)_4Ti$ are present, but because of the similar chemical shifts in **2** and **3** it seems less likely. The elemental analyses are consistent with the proposed constituents of **3**.

Chemical vapor deposition

To find a processing window for the CVD of $PbTiO_3$-, $PbZrO_3$- and $Pb(Zr_{1-x}Ti_x)O_3$-films, initially, the deposition behavior of **2**, **3** and **4** as a function of substrate-temperature was examined. Fig. 4 shows the deposition rate *vs.* deposition temperature of **4** at a constant precursor flow of 0.4×10^{-1} mbar.

We observed the highest deposition rates at temperatures around 400 °C. Below 300 °C nearly no deposition occurred. Over 600 °C, we observed no deposition on the substrates but on the colder ambient parts of the CVD reactor, like on glass and on stainless-steel parts. Optimal parameters for the deposition of dense $PbTiO_3$, $PbZrO_3$ and $Pb(Zr_{1-x}Ti_x)O_3$ films were found to be a precursor flow of 0.6×10^{-1} mbar at 410 °C. Thus, deposition rates up to 4 nm min^{-1} were achieved.

Chemical vapor deposition of 4 ($Et_3Pb(O^tBu)_5Ti/Et_3Pb(O^tBu)_5Zr$)

After deposition of PZT at 410 °C on Pt/Ti/SiO_2/Si-substrates, the films were RTA-treated to form a perovskite phase. To examine the influence of the annealing temperature, the films were treated by rapid thermal annealing (RTA) at 550 °C, 600 °C, 650 °C, 700 °C, and 750 °C for 5 min in ambient oxygen. In Fig. 5, XRD patterns of deposited PZT films after RTA treatment are shown.

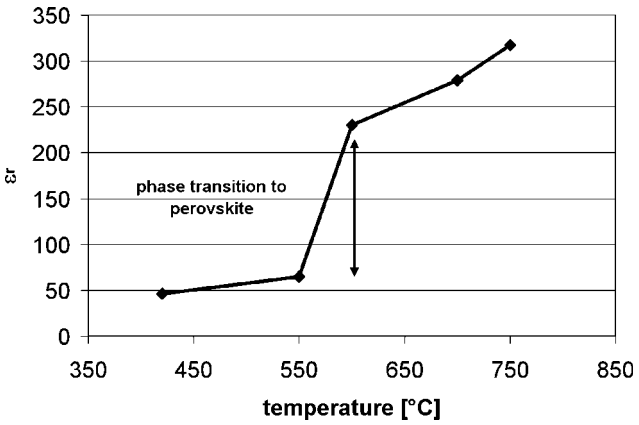

Fig. 6 Characteristics of the dielectric constant ε_r depending on the annealing temperature.

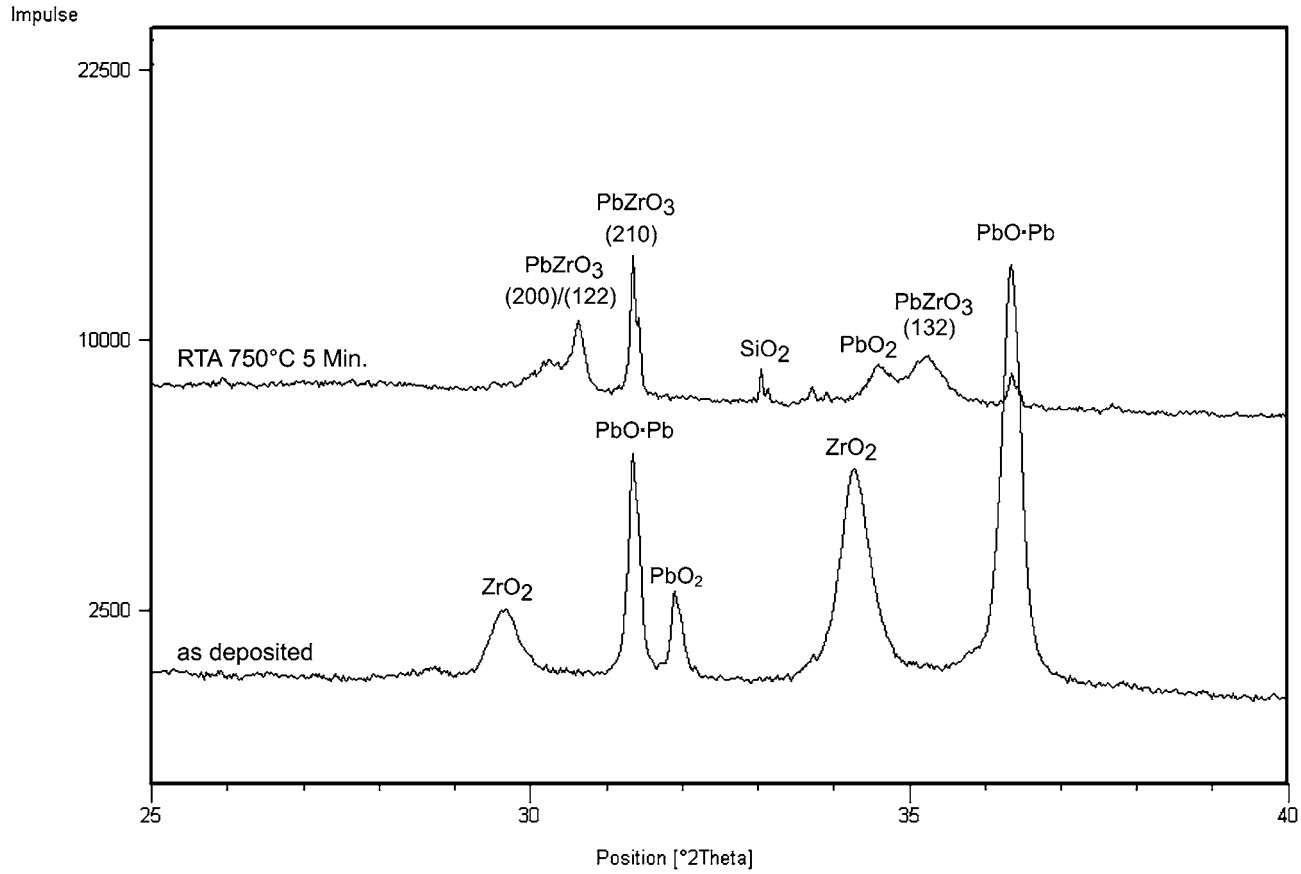

Fig. 7 XRD patterns of the deposited $PbZrO_3$ films on silicon substrate before and after RTA treatment (5 min, 750 °C).

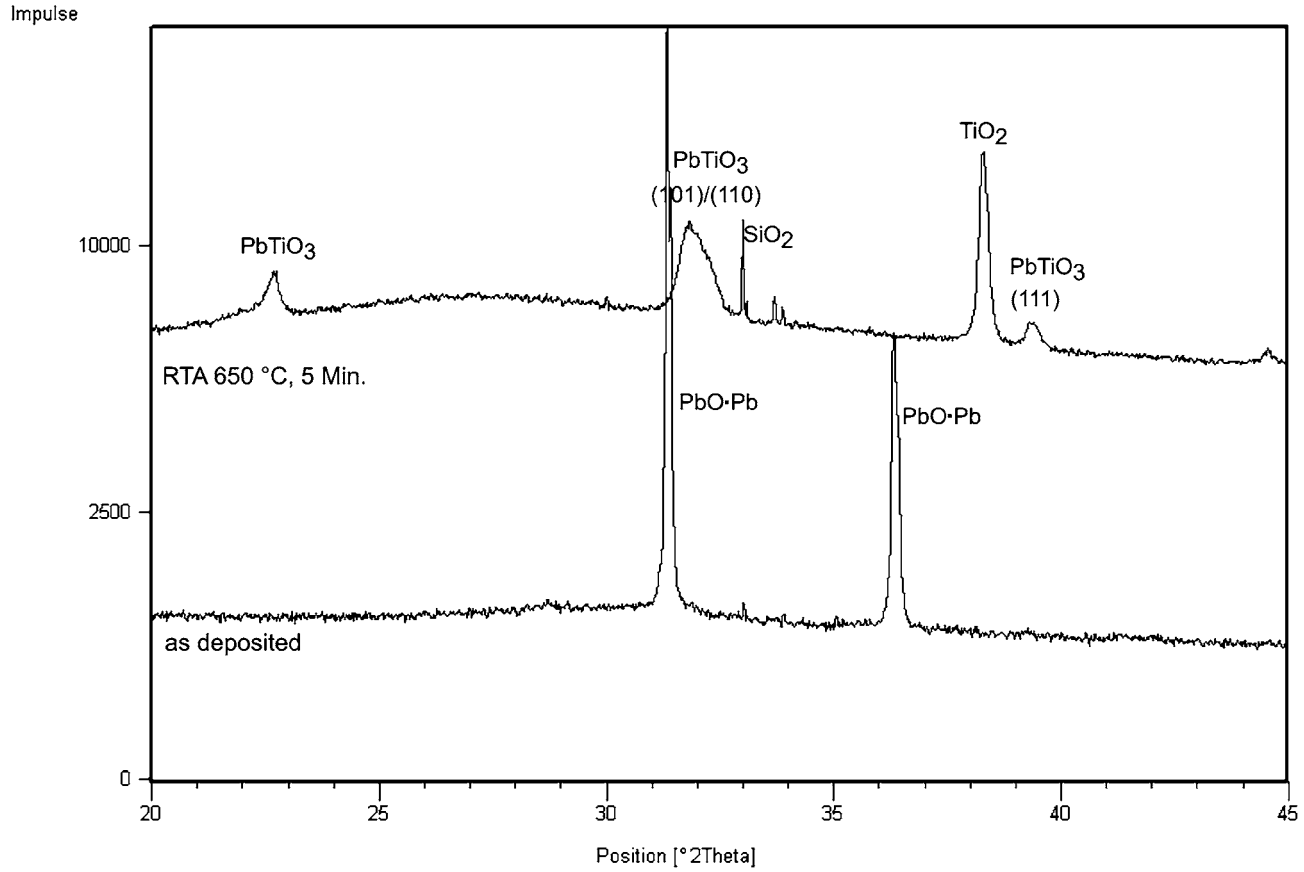

Fig. 8 XRD patterns of the deposited $PbTiO_3$ films on silicon substrate before and after RTA treatment (5 min, 650 °C).

The as-deposited films show no crystallinity. For the 550 °C treated film, besides the perovskite phase, a small pyrochlore[29] peak was detected at $2\theta = 29°$. For the complete formation of the perovskite phase, the films were annealed above 650 °C. At 700 °C the perovskite phase was fully developed with a (100) preferred orientation (Fig. 5).

Fig. 6 shows the characteristics of the dielectric constant ε_r, measured by a precision LCR Meter depending on the annealing temperature. We assigned the jump at 600 °C from 50 to 230 in ε_r to the perovskite transition. Depending on the film composition, we measured relatively low values up to 450 for the dielectric constant ε_r. This property could be interesting in the field of ultrasonic transducers regarding impedance matching.

Chemical vapor deposition of 2

$PbZrO_3$ films were deposited at 500 °C on silicon wafers. After deposition we observed a film consisting of several oxide phases of lead and zirconium of which we could determine PbO, PbO_2 and ZrO_2 from XRD. In the EDX spectrum we could find Zr, Pb, oxygen together with Si from the substrate. No other elements can be detected. To form the orthorhombic $PbZrO_3$-phase, the films were RTA-treated at 750 °C for 5 min. Fig. 7 shows the XRD patterns before and after the thermal treatment. Besides the substrate peaks, we observed an orthorhombic $PbZrO_3$-phase and a small peak for lead(IV) oxide (PbO_2) at $2\theta = 34.5°$.

Chemical vapor deposition of 3

$PbTiO_3$ films were deposited at 350 °C on silicon wafers. After deposition we observed a film consisting of several oxide phases of

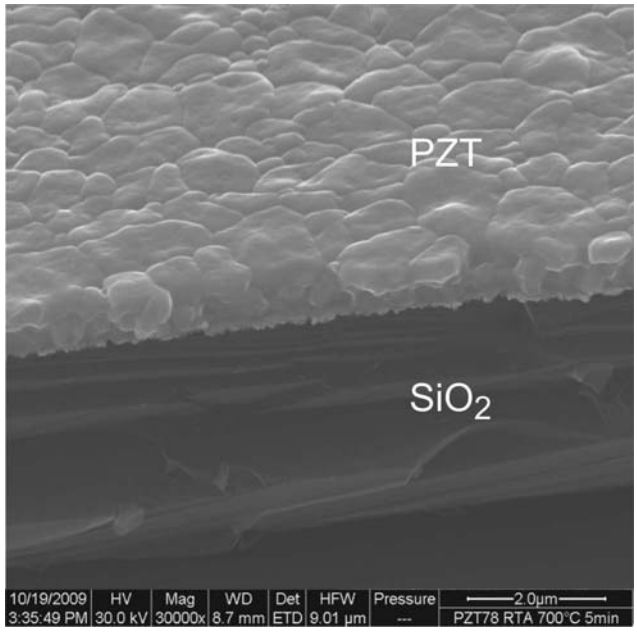

Fig. 9 SEM image of a cross-sectional view of a $Pb(Zr_{1-x}Ti_x)O_3$ film on $Pt/Ti/SiO_2/Si$-substrate, RTA-treated at 700 °C for 5 min.

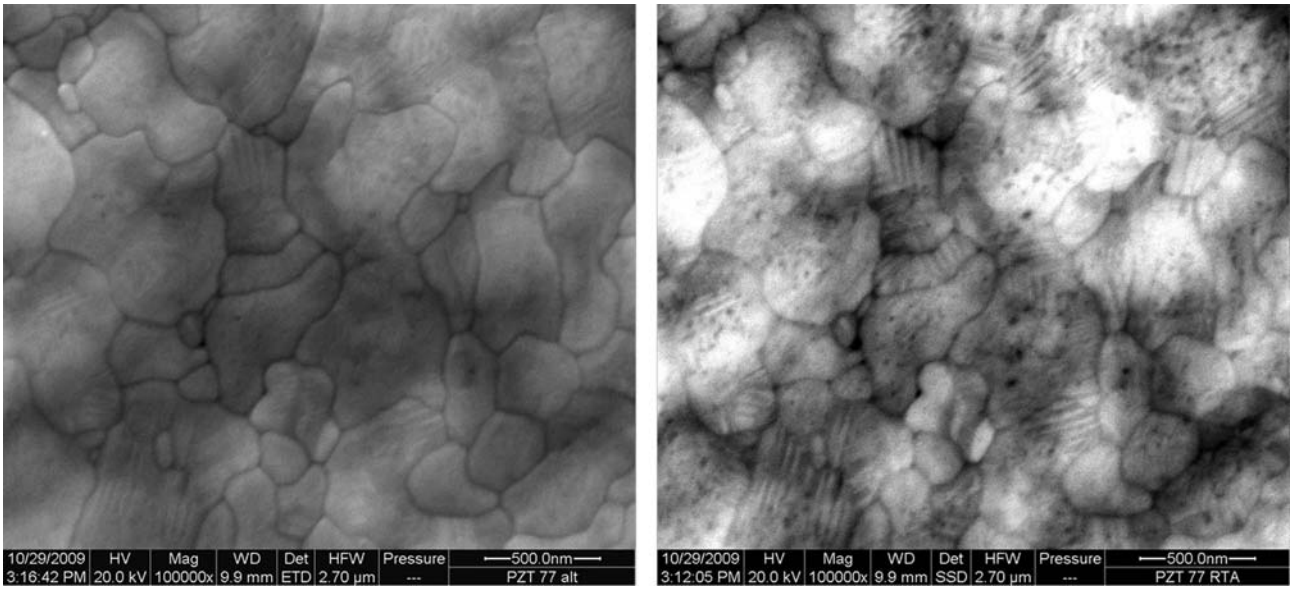

Fig. 10 SEM images (top view) of the microstructure of the $Pb(Zr_{1-x}Ti_x)O_3$ film after RTA treatment at 700 °C for 5 min. Left: secondary electrons contrast, right: backscattered electrons contrast. Grain size: 100 nm–500 nm.

lead (PbO, Pb·PbO) and titanium (TiO_2). To form the tetragonal $PbTiO_3$-phase, the films were RTA-treated at 650 °C for 5 min. Fig. 8 shows the XRD patterns before and after the thermal treatment. Besides the substrate peaks, we observed a tetragonal $PbTiO_3$-phase and a peak for titanium oxide (TiO_2) at $2\theta = 38.5°$.

SEM Analysis of the deposited PZT films

After heat treatment, the PZT films obtained from $(Et_3Pb(O^tBu)_5Zr$ and $Et_3Pb(O^tBu)_5Ti$ (**4**) show a smooth surface with grain sizes between 100 nm and 500 nm (Fig. 9).

Moreover, it was possible to make domain structures visible using backscattered electrons for contrast in SEM.

Fig. 10 shows SEM images of the same area (top view) of a PZT film in secondary electrons contrast (left) and backscattered electrons contrast (right). We could observe domains inside the grains and overlapping the grains with 90° Bloch walls.

Lattice parameters and composition of the deposited films

During XRD analysis we found a shift of the peaks depending on the composition of the quasi-single-source precursor (**4**). After comparing the Zr/Ti-ratio before and after the CVD process, we observed a loss of $PbZrO_3$ in a range of nearly 10% during the CVD. We assume that the higher decomposition tendency of the lead zirconate precursor is responsible for that behavior. Therefore, we had to add an excess of 10% $Et_3Pb(O^tBu)Zr(O^tBu)_4$ to the starting single-source precursor compound **4**, to obtain the desired stoichiometry.

Fig. 11 shows the characteristics of the lattice parameters *a* and *c* depending on the film composition. Besides XRD analysis using the Rietveld algorithm, we also checked the contamination of the films by EDX.

According to the literature,[30] lattice parameter *c* increases at higher $PbTiO_3$ concentrations, while lattice parameter *a* decreases.

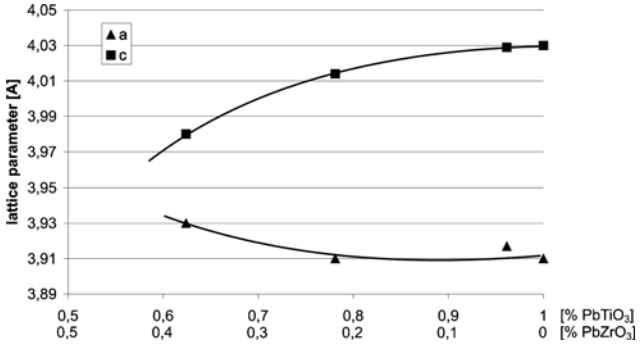

Fig. 11 Lattice parameters of the deposited PZT films with respect to Ti/Zr ratio.

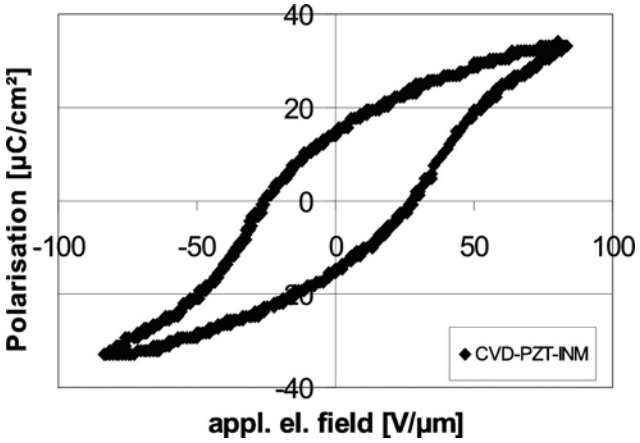

Fig. 12 Hysteresis loop of PZT films obtained by the single-source CVD-process.

Electrical characterization of the films

After the films were patterned and the top electrode was sputtered on, hysteresis loops were measured by use of a classical

Sawyer–Tower circuit.[24,27] Fig. 12 shows the hysteresis loop of PZT films in the sub-µm range produced by the single-source CVD process. We observed considerably good ferroelectric properties for the films obtained by CVD. The remnant polarization of the films exhibits 15–20 µC cm^{-2}. The coercive field strength of the CVD films shows high values with 25 V $µm^{-1}$.

Conclusions

The synthesis of the mixed metal species $Et_3Pb(O^tBu)Zr(O^tBu)_4$ (**2**) and $Et_3Pb(O^tBu)Ti(O^tBu)_4$ (**3**) by reaction between the amides $Zr(NEt_2)_4$, $Ti(NEt_2)_4$ and $Et_3PbN(SiMe_3)_2$, respectively, (**1**) in the presence of *tert*-butyl alcohol has been achieved. Almost identical properties and complement miscibility of **2** and **3** resulted in a volatile quasi single-source precursor (**4**) suitable for the deposition of $Pb(Zr_{1-x}Ti_x)O_3$ thin-films in a classical thermal CVD process. In this context, **3** represents the first well-characterized volatile mixed metal species having a stoichiometry Pb : Ti = 1 : 1. After chemical vapor deposition at around 400 °C on Pt/Ti/SiO_2/Si-substrates and thermal treatment at temperatures around 650 °C, transparent $PbTiO_3$-, $PbZrO_3$- as well as $Pb(Zr_{1-x}Ti_x)O_3$ thin films with thicknesses up to 1 µm have been obtained. PZT films with a smooth surface morphology show a (100) oriented perovskite phase, a remnant polarization of 20 µC cm^{-2} and a comparatively high coercive field strength of 20 V $µm^{-1}$. The synthesized single-source precursors **2** and **3** are promising candidates to replace common precursors for the fabrication of PZT materials in the near future.

References

1 M. M. Zhang, Z. Jia and T. L. Ren, *Solid-State Electron.*, 2009, **53**, 473.
2 S. Li, X. Wu and L. Zhang, *J. Electroceram.*, 2008, **21**, 520.
3 A. P. Wilkinson, J. S. Speck and A. K. Cheetham, *Chem. Mater.*, 1994, **6**, 750.
4 D. M. Kim and C. B. Eom, *Appl. Phys. Lett.*, 2006, **88**, 142904.
5 H. Hu, C. J. Peng and S. B. Krupanidhi, *Thin Solid Films*, 1993, **223**, 327.
6 D. Remiens, E. Cattan, C. Soyer and T. Haccart, *Mater. Sci. Semicond. Process.*, 2003, **5**, 123.
7 R. W. Schwartz, *Integr. Ferroelectr.*, 1995, **7**, 259.
8 H. Yamazaki, T. Tsuyama, I. Kobayashi and Y. Sugimori, *Jpn. J. Appl. Phys.*, 1992, **31**, 2995.
9 D. H. Kim, J. S. Na and S. W. Rhee, *J. Electroceram. Soc.*, 2001, **10**, 148.
10 Y. M. Kim, W. J. Lee and H. G. Kim, *Thin Solid Films*, 1996, **279**, 140.
11 I. S. Chen, J. F. Roeder, T. E. Glassman and T. H. Baum, *Chem. Mater.*, 1999, **11**, 209.
12 W. C. Hendricks, S. B. Desu and C. H. Peng, *Chem. Mater.*, 1994, **6**, 1955.
13 R. A. Assink and R. W. Schwartz, *Chem. Mater.*, 1993, **5**, 511.
14 I. Bretos, R. Jiménez, J. Garcia-López, L. Pardo and M. L. Calzada, *Chem. Mater.*, 2008, **20**, 5731.
15 M. Veith, *J. Chem. Soc., Dalton Trans.*, 2002, 2405.
16 M. Veith, S. Mathur and C. Mathur, *Polyhedron*, 1998, **17**(5–6), 1005.
17 M. Veith, A. Altherr and H. Wolfanger, *Adv. Mater.*, 1999, **5**, 87.
18 M. Veith, S. Mathur, V. Huch and T. Decker, *Eur. J. Inorg. Chem.*, 1998, 1327.
19 D. J. Teff, J. C. Huffman and K. G. Caulton, *Inorg. Chem.*, 1995, **34**(10), 2491.
20 D. J. Teff, J. C. Huffman and K. G. Caulton, *Inorg. Chem.*, 1996, **35**, 2981.
21 S. Daniele, R. Papiernik and L. G. Hubert-Pfalzgraf, *Inorg. Chem.*, 1995, **34**, 628.
22 L. Ma and D. A. Payne, *Chem. Mater.*, 1994, **6**(7), 875.
23 B. A. Vaartstra, *US-Patent US005326892A*, 1994.
24 D. C. Bradley and I. M. Thomas, *J. Chem. Soc.*, 1960, 3857.
25 F. Vasilliu, G. J. Norga, L. Fe, D. Wounters and D. Van Der Biest, *J. Optoelectron. Adv. Mater.*, 2003, **5**(3), 777.
26 K. Zheng, J. Lu and J. Chu, *Jpn. J. Appl. Phys.*, 2004, **43**(6b), 3934.
27 C. B. Sawyer and C. H. Tower, *Phys. Rev.*, 1930, **35**, 269.
28 T. Lehnert, J. Adam and M. Veith, *J. Appl. Phys.*, 2009, 106.
29 M. T. Weller, R. W. Hughes, J. Rooke, C. S. Knee and J. Reading, *Dalton Trans.*, 2004, 3032.
30 J. Puchalla, *Schriften des Forschungszentrums Jülich, Reihe Informationstechnik*, 2007, Band 17, ISSN 1433-5514.

